

# DESIGN AND OPTIMIZATION OF AIR-ASSISTED SPIRAL SEED-SUPPLY DEVICE FOR HIGH-SPEED DENSE PLANTING MAIZE SEEDER

## 玉米高速密植播种机气送式螺旋供种装置设计与优化

Wen-sheng SUN <sup>1)</sup>, Shu-juan YI <sup>1)</sup>, Hai-long QI <sup>2)</sup>, Yi-fei LI <sup>1,3)</sup>, Zhi-bo DAI <sup>1)</sup>, Yu-peng ZHANG <sup>1)</sup>,  
Jia-sha YUAN <sup>1)</sup>, Song WANG <sup>1)</sup>

<sup>1)</sup>College of Engineering, Heilongjiang Bayi Agricultural University, Daqing/P.R.China

<sup>2)</sup>Heilongjiang Beidahuang Modern Agricultural Service Group Zhongrong Agricultural Machinery Co., Ltd, Harbin / P.R.China

<sup>3)</sup>College of Engineering, Northeast Agricultural University, Harbin/P.R.China

Tel: +86-459-13836961877; E-mail: yishujuan\_2005@126.com

Corresponding author: Shu-juan Yi

DOI: <https://doi.org/10.35633/inmateh-75-01>

**Keywords:** maize, seed-supply device, air-assisted, spiral, CFD

### ABSTRACT

In order to improve the seed supply performance of high-speed dense planting maize seeder, an air-assisted spiral seed-supply device was designed and optimized. The kinetic model of maize seeds in the migration zone was established. Based on computational fluid dynamics (CFD) simulation, the pressure and velocity distribution in the axial plane were explored when the blower pressure was 4.0, 4.5, 5.0, 5.5, 6.0 kPa, respectively. A two-factor, five-level central composite design (CCD) experiment was conducted using blower pressure and spiral shaft rotational speed as test factors while seed supply rate, coefficient of variation of seed supply rate stability and seed breakage rate were selected as seed supply performance indicators. The influence trends of the interaction terms on these performance indicators were explored. Based on the multi-objective variable optimization method, the optimal working parameter combination of the air-assisted spiral seed-supply device was determined and verified by bench experiments. The results showed that the optimal combination of working parameters was a blower pressure of 6.0 kPa and a spiral shaft rotational speed of 80 r/min. Under the verification test, the seed supply rate, the coefficient of variation of seed supply rate stability and the seed breakage rate were 2933.21 g/min, 1.87 % and 1.69 %, respectively, with a relative error of less than 5.5% compared to the optimized results. This study can provide a reference for the optimized design of seed-supply devices for high-speed dense planting seeders.

### 摘要

为提高玉米高速密植播种机供种环节的供种性能, 设计并优化了一种气送式螺旋供种装置。建立了玉米种子在迁移区的动力学模型。基于 CFD 仿真探究了气流送种区在风机压力分别为 4.0、4.5、5.0、5.5、6.0 kPa 时中轴面的压强与流速分布。以风机压力、螺旋轴转速为试验因素, 以供种速率、供种速率稳定性变异系数、种子破损率为供种性能指标进行了二因素五水平的中心组合设计试验, 探究了因素的交互项对供种速率、供种速率稳定性变异系数、种子破损率的影响趋势。基于多目标变量优化的方法确定了气送式螺旋供种装置的最佳工作参数组合并进行了试验验证。结果表明: 装置的最佳工作参数组合为风机压力 6.0 kPa、螺旋轴转速 80 r/min, 验证试验下该参数组合的供种速率、供种速率稳定性变异系数、种子破损率分别为 2933.21 g/min、1.87 %、1.69 %, 与参数优化结果相对误差在 5.5 % 以内。本研究可为高速密植播种机供种装置的优化设计提供参考。

### INTRODUCTION

Maize is one of the most widely planted and productive food crops in the world (Tang et al., 2024; Fanigliulo et al., 2022). With the increasing demand for feed raw materials and the rapid development of deep-processing industry, the demand for maize in China has expanded rapidly (Huai et al., 2024). To improve maize yield, the dense planting pattern has gained widespread attention among agricultural workers. Maize densification planting mode (Sun et al., 2024) is based on the precision sowing technology, which can reasonably reduce the seed spacing of maize. That not only ensures the space for plant growth, but also improves the planting density and increase production and efficiency. But in the dense planting mode, the

<sup>1</sup>Wen-sheng Sun, Ph.D.; Shu-juan Yi, Prof. Ph.D.; Hai-long Qi, bachelor degree; Yi-fei Li, Ph.D.; Zhi-bo Dai, master degree; Yu-peng Zhang, master degree; Jia-sha Yuan, master degree; Song Wang, Ph.D.

sowing quantity per unit area of soil will increase, the seed spacing will decrease, and the sowing frequency of the seeder will also be higher during high-speed operation. In addition, maize seeds are often coated before sowing, and damage to the seed coating skin should be avoided during the sowing process.

At present, the seed box of the seeder used for conventional operation is generally not provided with a seed supply control unit, and the seed is quantitatively supplied according to the outlet structure size of the seed box (Ding et al., 2021). The seed supply device of the centralized pneumatic dense planting seeder is mainly controlled by machinery, and the sowing speed is generally below 10 km/h. When the seed supply device operates at a high speed (above 10 km/h), it is easy to appear the phenomenon of "lack of power" of seed supply (Wang et al., 2021; Wang et al., 2020). Gao Xiaojun et al., (2022), explored a quantitative feeding device with a staggered symmetrical spiral groove wheel based on the discrete element method (DEM), and analyzed the effects of different inclination angles and lengths of the grooved wheels on the uniformity of maize particles flow. Yuan Hao et al., (2020), designed a piezoelectric vibration seed supply device to improve the seeding performance of low seeding capacity seed-metering device for plug seedling of super hybrid rice, and explored the influence law of seed tank depth and amplitude on seed supply performance based on DEM. Lei Xiaolong et al., (2017), explored the effects of dimple depth, dimple pitch and length of pressurized tube on the seed distribution and seeding uniformity during the seed supply stage of the air-assisted centralized planter, and optimized the structural parameters of the pressurized tube. Gao Xiaojun et al. (2018) investigated the changing rules of fluid field, coupling field, and particle field of venturi feeding tube under different nozzle mouth shrinkage angles, and optimized the constriction angle. However, there is little research on the seed-supply link of maize dense planting seeder under high-speed operation.

In order to improve the seed supply performance of seed-supplying link of high-speed dense planting seeder of maize, an air-assisted spiral seed-supply device with spiral seed relocation and airflow seed delivery was designed and optimized. The theoretical model of maize seeds in the migration zone of the device was established, and the airflow distribution of the airflow seed delivery zone under different blower pressures was explored by computational fluid dynamics (CFD) simulation. The optimal working parameter combination of the device was obtained through the central composite design (CCD) test of two factors and five levels. The seed supply performance of the device was further improved.

## MATERIALS AND METHODS

### Overall structure and working principle

The high-speed dense planting seeder of maize can complete the continuous operation links such as stubble cleaning, ditching, sowing, pressing and soil-covering at one time. As the seed-supply unit of the sowing link (Sun et al., 2024), the air-assisted spiral seed-supply device is mainly composed of a blower, an inlet pipe, an outlet pipe, a pipe, a seed box, a spiral shaft, a sleeve, a motor, a seed-supply nozzle and other parts. The seeds in the seed box have to undergo three processes of migration, mixing and conveying in the device, which can be divided into two parts of the migration zone and the airflow seed delivery zone according to the working process. As the medium connecting the seed box and the airflow seed delivery zone, the migration zone is the core unit of the device. The spiral shaft and the sleeve are the main components of the migration zone, and the hollow part between the spiral shaft and the sleeve accommodates the migration movement of the maize seeds. The spiral shaft parameters include spiral shaft outer diameter  $D_1$  of 56 mm, inner diameter  $d_1$  of 19 mm, guide  $P_t$  of 56 mm, etc. The sleeve parameters include opening angle  $\varphi$  of  $180^\circ$ , sleeve length  $L_1$  of 145 mm, sleeve axial opening  $L_2$  of 45 mm, sleeve outer diameter  $D_2$  of 63 mm, etc.

As shown in Fig.1, the maize seeds in the seed box fall from the seed inlet to the migration zone by gravity, and orderly migrate towards the airflow seed delivery zone under the push of the spiral blades. Following the principle of "first come, first out", they fall from the seed outlet of the migration zone to the airflow seed delivery zone. The motor drives the spiral shaft to rotate clockwise at an angular velocity of  $\omega$ , and the spiral blades are left-handed. The edge of the spiral blades rises along the left arm. The migration amount of the seeds in the migration zone in unit time is adjusted by changing the rotational speed of the motor. The airflow generated by the blower flows in from the inlet pipe. The migrated seed cluster are mixed with the airflow in the seed-supply nozzle to form a gas-solid two-phase flow, and then flows into the seed-metering device through the outlet pipe and the pipe. The conveying velocity of the seeds in the airflow seed delivery zone is changed by adjusting the blower pressure. By adjusting the rotational speed of spiral shaft and the blower pressure, the aim of precisely adjustable and efficient seed-supply of the device is achieved, and the seed supply operation requirement on the device when the maize dense planting seeder operates at a high speed is met.

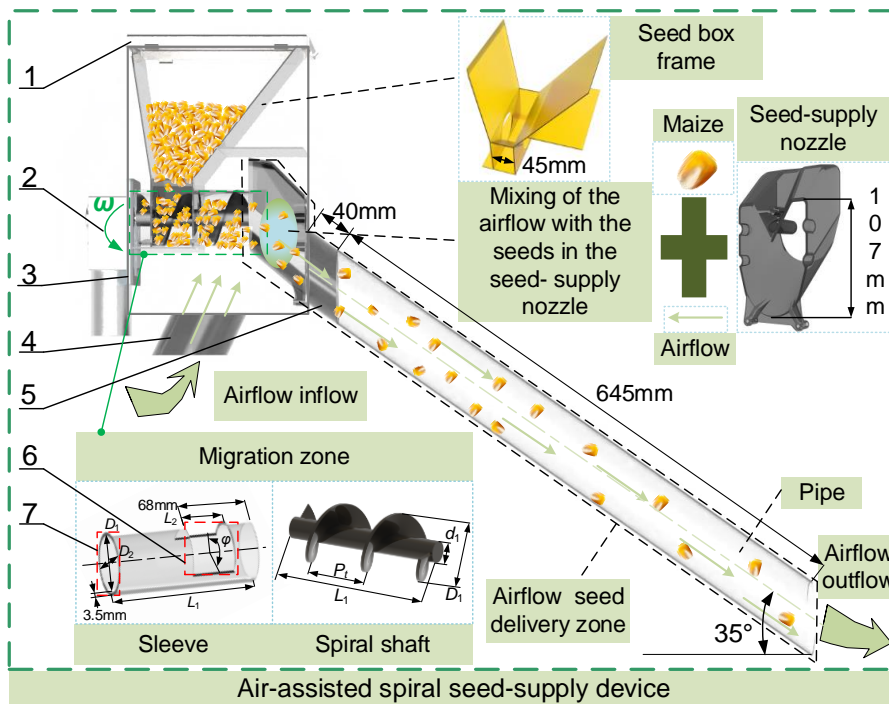


**Fig. 1 - Overall structure and working principle**

1. seed box cover; 2. motor; 3. seed box; 4. inlet pipe; 5. outlet pipe; 6. seed inlet of migration zone; 7. seed outlet of migration zone.

**Analysis of the seed-supply process in the migration zone**

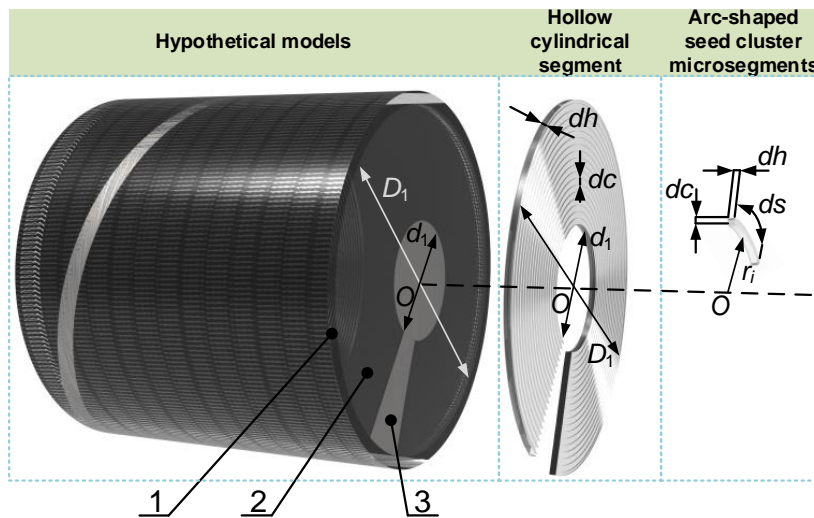


**Fig. 2 - Theoretical assumptions of the seed supply process**

1. sleeve; 2. seed cluster; 3. spiral shaft.

After the seeds flow into the migration zone from the seed box, they will complete the migration process in the form of bulk particles under various forces such as gravity, inertia, friction and so on. Due to the great difference in the shape and size of maize seeds, in order to facilitate the theoretical analysis of the seed cluster in the migration zone, the following motion assumptions are established for the stable seed supply process of maize seeds in the migration zone based on the infinitesimal method (Yao *et al.*, 2022):

(1) Seed cluster in the migration zone are filled completely in the hollow between the spiral shaft and the sleeve, the phenomena of separation, jumping and other like cannot occur, and the seed cluster are tightly attached to the spiral blade;

(2) Seed cluster are axially divided among the spiral blades into uniform and complete seed cluster segments, where in each segment is a hollow cylindrical segment which take the center O of a spiral shaft as a circle center, has the same inner diameter as the inner diameter of the spiral shaft, has the same outer diameter as the outer diameter of the spiral shaft and has the thickness of  $dh$ , and radially dividing each hollow cylindrical segment into arc-shaped seed cluster microsegments with the length of  $dc$ ;

(3) The arc-shaped seed cluster microsegment  $ds$  at any radius  $r_i$  on the radial section of any spiral shaft is taken as the research object, and the microsegment section is a rectangle of  $dc \times dh$ , as shown in Fig.2. The rotational speed of the adjacent annular seed cluster microsegments diffusely distributed in any radial direction will change.

The spiral shaft of the device is a standard single-head screw with equal guide and equal diameter. The spiral blade exerts a force on the seed cluster, which makes the seed cluster produce a migration motion, in which the rotation of the spiral shaft is induced motion, and the motion of the seed cluster relative to the spiral blade is relative motion. The seed cluster forms a complex composite motion under these two motions. A dynamic analysis is performed on the migration process of the seed cluster microsegments clinging to any radius  $r_i$  of the middle segment of the spiral blade, and a spatial rectangular coordinate system is established with the center of mass of the seed cluster microsegments as the coordinate origin, the axial direction of the spiral shaft as the  $z$  axis, the radial direction as the  $x$  axis, and the tangential direction as the  $y$  axis, as shown in Fig.3.

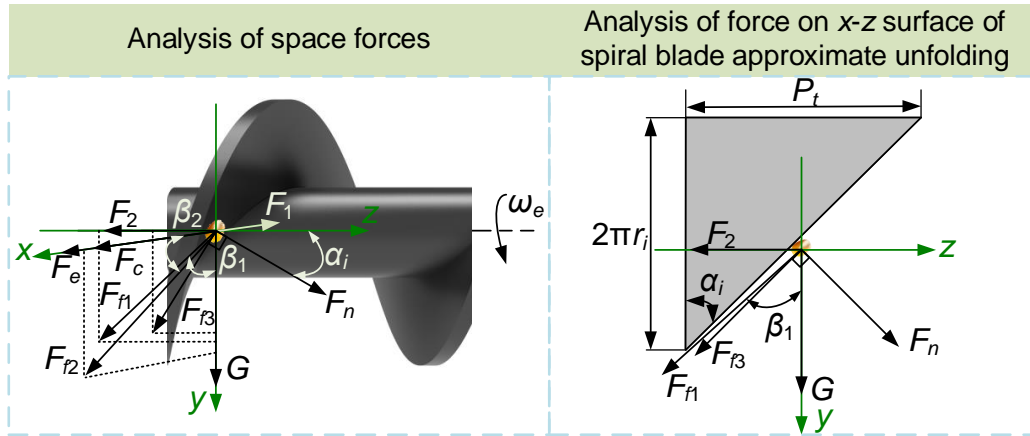


Fig. 3 - Dynamic analysis of seed cluster microsegments

The force acting on the seed cluster microsegments during the rotation of the spiral shaft can be divided into a supporting force  $F_n$  perpendicular to the spiral blade and a friction force  $F_{f3}$  between the seed and the spiral blade. In the process of seed movement, the microsegments will have the trend of moving axially to the seed outlet and radially outward. According to Newton's third law of motion-force and acceleration, the microsegments will be subjected to the interaction forces  $F_1$  and  $F_2$  of the adjacent seed cluster microsegments in the radial and axial directions, and at the same time, the moving microsegments will generate additional friction forces  $F_{f1}$  and  $F_{f2}$  due to the forces  $F_1$  and  $F_2$ . In addition, because the motion of the microsegment is a composite motion composed of relative motion and induced motion, and the induced motion is rotation, the inertial centrifugal force  $F_e$  and the Coriolis force  $F_c$  should be considered when analyzing the force model of the microsegment. According to the basic equation of particle relative motion dynamics, the microsegment dynamics equation is established as follows:

$$\left\{ \begin{array}{l} ma_r = F_e + F_c + F \\ F_e = mr_i\omega_e^2 \\ F_c = 2mr_i\omega_e\omega_r \\ \omega_a = \omega_e - \omega_r \\ F_{f1} = \mu_2F_1 \\ F_{f2} = \mu_2F_2 \\ F_{f3} = \mu_1F_n \\ G = mg \\ \tan \alpha_i = \frac{P_t}{2\pi r_i} \end{array} \right. \quad (1)$$

where:  $m$  is the mass of the microsegment, (kg);  $\alpha_r$  is the relative acceleration of the microsegment, ( $m \cdot s^{-2}$ );  $\omega_a$  is the absolute angular velocity of the microsegment, (rad/s);  $\omega_e$  is the angular velocity of the spiral shaft, (rad/s);  $\omega_r$  is the angular velocity of the microsegment relative to the spiral shaft, (rad/s);  $\mu_1$  is the friction coefficient between spiral blade and seed;  $\mu_2$  is the friction coefficient between the seeds;  $G$  is the gravity exerted on the microsegment, (N);  $g$  is the acceleration of gravity, ( $m \cdot s^{-2}$ );  $\alpha_i$  is the helix angle at the position of the spiral shaft where the microsegment are located, ( $^\circ$ ).

Projecting the relative acceleration  $\alpha_r$  to the x-axis, y-axis and z-axis, the rectangular coordinate form of the seed relative motion differential equation is

$$\begin{cases} m \frac{d^2 r_x}{dt^2} = m \frac{dv_x}{dt} = ma_{r-x} = F_c + F_e + F_{f2} \cos \beta_2 - F_1 \\ m \frac{d^2 r_y}{dt^2} = m \frac{dv_y}{dt} = ma_{r-y} = G + F_{f1} \cos \beta_1 + F_{f3} \cos \alpha_i + F_n \sin \alpha_i + F_{f2} \sin \beta_2 \\ m \frac{d^2 r_z}{dt^2} = m \frac{dv_z}{dt} = ma_{r-z} = F_n \cos \alpha_i - F_{f3} \sin \alpha_i - F_{f1} \sin \beta_1 - F_2 \end{cases} \quad (2)$$

where:

$\alpha_{r-x}$  is the projection of the relative acceleration of the microsegment on the x-axis, ( $m \cdot s^{-2}$ );  $\alpha_{r-y}$  is the projection of the relative acceleration of the microsegment on the y-axis, ( $m \cdot s^{-2}$ );  $\alpha_{r-z}$  is the projection of the relative acceleration of the microsegment on the z-axis, ( $m \cdot s^{-2}$ );  $\beta_1$  is the angle between the friction force  $F_{f1}$  and the gravity  $G$ , ( $^\circ$ );  $\beta_2$  is the angle between the friction force  $F_{f2}$  and the positive x-axis, ( $^\circ$ ).

The relative accelerations of the microsegment in the x-, y-, and z-axes are

$$\begin{cases} a_{r-x} = r_i \omega_r^2 \\ a_{r-y} = 0 \\ a_{r-z} = 0 \end{cases} \quad (3)$$

Simultaneous (1-3), available:

$$\frac{mr_i[(2\omega_e - \omega_a)^2 - 2(\omega_e - \omega_a)^2] = F_1[1 - T\mu_2 \sin \beta_2 - \mu_2 \cos \beta_2 (T\mu_2 \cos \beta_1 - \mu_2 \sin \beta_1)] - T\mu_2 mg \cos \beta_2}{1 - T\mu_2 \sin \beta_2} \quad (4)$$

which:

$$\begin{cases} T = \frac{\mu_1 \sin \alpha_i - \cos \alpha_i}{\mu_1 \cos \alpha_i + \sin \alpha_i} \\ \sin \alpha_i = \frac{P_t}{\sqrt{P_t^2 + (2\pi r_i)^2}} \\ \cos \alpha_i = \frac{2\pi r_i}{\sqrt{P_t^2 + (2\pi r_i)^2}} \end{cases} \quad (5)$$

It can be seen from the formula (4) that the absolute angular velocity  $\omega_a$  is related to the angular velocity  $\omega_e$ , the radius  $r_i$ , and the guide  $P_t$ . When the angular velocity  $\omega_e$  is constant, the absolute angular velocity  $\omega_a$  will change with the radius  $r_i$  of the microsegment location, which is consistent with the motion assumption in the previous content. Studies have shown (Chen *et al.*, 2015; Yang *et al.*, 2020) that when the rotational speed of the spiral shaft is too fast, the seed cluster near the inner diameter of the spiral shaft will produce an additional seed-cluster-flow, which will jump and roll in the radial direction and affect the axial motion of the seed cluster. In addition, if the rotational speed is too fast, the seeds just leaving the migration zone will splash around due to the excessive inertial force. The maximum inertial centrifugal force of the seeds should be less than the gravity of the seeds to ensure a smooth transition from the migration zone to the airflow seed delivery zone:

$$m\omega_{max}^2 \frac{D_1}{2} \leq K_1 mg \Rightarrow n_{max} \leq \frac{30K_1}{\pi} \sqrt{\frac{2g}{D_1}} \quad (6)$$

where:

$\omega_{max}$  is the limiting angular velocity of the spiral shaft, (rad/s);  $n_{max}$  is the limiting rotational speed of the spiral shaft, (r/min);  $K_1$  is the reliability coefficient.

### Simulation based on CFD

The UG NX 12.0 software is used to draw the fluid domain model and import it into Space Claim software for correction. The corrected model is imported into Fluent Meshing module for meshing. The minimum and maximum values of the surface grid are set to 0.5 mm and 5 mm, respectively. After the surface grid is generated, the fluid domain is calculated using polyhedral grid to fill the body grid. The fluid domain model is shown in Fig. 4.

According to the characteristics of the gas flow in the device, the standard K-epsilon model is used as the turbulence model, the second-order upwind equation is used as the momentum equation, the first-order upwind equation is used for the turbulent kinetic energy and the turbulent dissipation rate, the turbulent intensity is set to be 5 %, the turbulent viscosity ratio is set to be 10. The Fluent time-step is  $1 \times 10^{-3}$ s, and the total simulation time is 2 s. The inlet pressure was set as 4.0, 4.5, 5.0, 5.5, 6.0 kPa, respectively, and the outlet pressure was set as 0 Pa to explore the airflow distribution in the airflow seed delivery zone under different blower pressures.

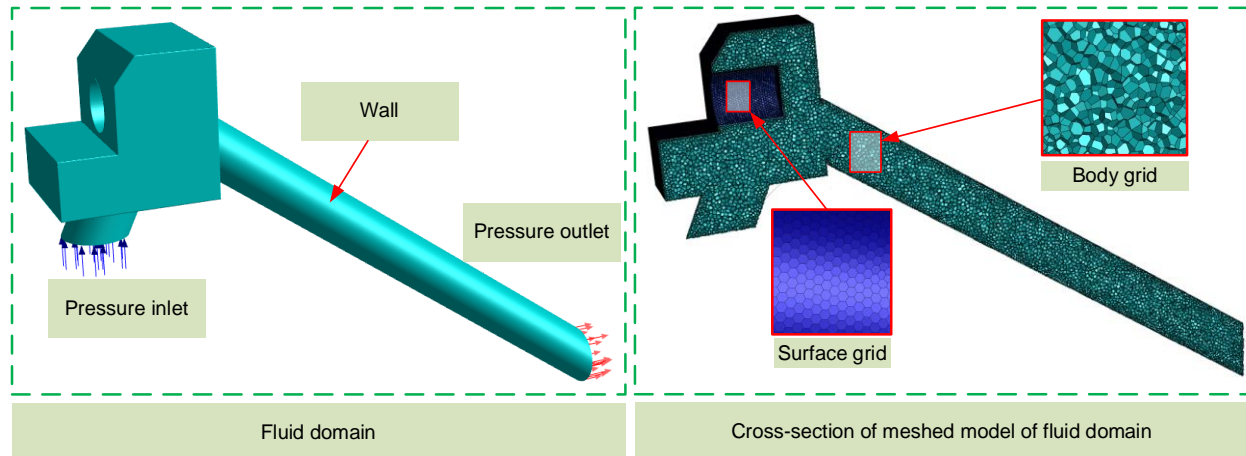


Fig. 4 - Establishment of CFD simulations

### Bench test

In June 2024, the bench test of the air-assisted spiral seed-supply device was carried out in the high-speed precision seeding laboratory of the College of Engineering, Heilongjiang Bayi Agricultural University, Daqing City, Heilongjiang Province, China. The test conditions and results are shown in Fig. 5.



Fig. 5 - Bench test

1. electronic balance; 2. measuring cylinder; 3. DP2000 intelligent pressure and wind velocity air volume meter; 4. frequency converter;
5. HTB-multi-stage blower; 6. air tube; 7. switch power supply; 8. infinite speed control knob; 9. display screen; 10. motor;
11. inlet pipe; 12. seed box; 13. outlet pipe; 14. pipe; 15. seed net.

The main test equipment includes HTB-multi-stage blower, frequency converter, DP2000 intelligent pressure and wind velocity air volume meter, seed net, motor, infinite speed control knob, switch power supply, electronic balance, etc. The typical maize variety "Farley 1439" (small rounded) planted in Heilongjiang Province of China were selected as the test seeds, and the basic material characteristic parameters were shown in Table 1. The selected seeds were all coated and sorted, and the results were the average values after multiple measurements.

Table 1

Basic material characteristics of maize seed

| Variety name                | Seed picture  | Moisture content /% | Thousand grain weigh/g | Density /g·cm <sup>-3</sup> | Pile angle/(°) | Length mm | Width mm  | Thickness mm |
|-----------------------------|---|---------------------|------------------------|-----------------------------|----------------|-----------|-----------|--------------|
| Farley 1439 (small rounded) |  | 12.6                | 296.4                  | 1.122                       | 20.23          | 8.03±0.41 | 7.12±0.46 | 6.34±0.43    |

In order to determine the optimal working parameters of the device and explore the interaction between the blower pressure and the rotational speed of spiral shaft on the seed-supply performance, a multi-factor experiment with two factors and five levels was carried out based on the CCD method. According to the actual test conditions, the blower pressure at 4.0 ~ 6.0 kPa and the rotational speed of spiral shaft at 50.0 ~ 80.0 r/min was set. The test factor codes are shown in Table 2, where  $X_1$  and  $X_2$  are the factor code values of the pressure and the rotational speed respectively.

Table 2

Experimental factors and level codes in multi-factor experiments

| Coded values | Experimental factors |                             |
|--------------|----------------------|-----------------------------|
|              | $X_1$ / kPa          | $X_2$ / r·min <sup>-1</sup> |
| -1.414       | 4.0                  | 50.0                        |
| -1           | 4.29                 | 54.4                        |
| 0            | 5.0                  | 65.0                        |
| 1            | 5.71                 | 75.6                        |
| 1.414        | 6.0                  | 80.0                        |

Referring to GB/T 9478-2005 "Testing methods of sowing in lines", the test indexes were seed supply rate  $\vartheta_i$ , coefficient of variation of the seed supply rate stability  $CV$  and seed breakage rate  $K_1$ . Wherein, the seed supply rate is defined as the mass of the seeds flowing out of the device in unit time. The coefficient of variation of seed supply rate stability is defined as the percentage of the standard deviation of the seed supply rate to the average value of it at the same level of device parameter, measured many times to evaluate the uniformity of seed supply in the device. The seed breakage rate is defined as the percentage of the broken seed mass  $Z_1$  out of the total seed mass  $Z_n$  flowing out of the device in given time. The evaluation index expression of seed supply performance is as follows:

$$\left\{ \begin{array}{l} \vartheta_i = \frac{\sum_{i=1}^{N_1} G_i}{N_1} \\ CV = \sqrt{\frac{\sum_{i=1}^{N_1} (G_i - \vartheta_i)^2}{N_1 - 1}} \times 100\% \\ K_1 = \frac{Z_1}{Z_n} \times 100\% \end{array} \right. \quad (7)$$

where:  $G_i$  is the seed quality of the  $i$ -th test, (g);  $N_1$  is the number of experiments.

In the experiment, the seeds discharged from the device were collected using the seed net for 1 minute. The net weight was measured, and then the broken seeds were picked up and weighed. Each group of experiments was repeated 5 times, and the seed supply rate, the coefficient of variation of the seed supply rate stability and the seed breakage rate were calculated under different treatments.

## RESULTS AND DISCUSSIONS

### Simulation analysis of flow field in the airflow seed delivery zone

In order to explore the pressure distribution in the airflow seed delivery zone under different inlet pressures, the pressure nephogram in the axial plane of the fluid domain at 2 s was intercepted, as shown in Fig. 6 a ~ e. In the figure, the pressure distribution in the axial plane is similar for different inlet pressures, the pressure is higher in the area from the inlet of the inlet pipe to the inlet of the outlet pipe, the pressure in the outlet pipe and the pipe is lower, and negative pressure appears near the outlet pipe and the pipe inlet.

With the increase of the inlet pressure, the pressure range of the airflow seed delivery zone is gradually increased. The pressure ranges at 4.0, 4.5, 5.0, 5.5 and 6.0 kPa were -1271.52 ~ 3993.05, -1426.41 ~ 4558.55, -1693.46 ~ 4994.76, -1957.58 ~ 5525.13, -1950.10 ~ 5961.19 Pa, respectively.

Dividing the segment of the flow field of the axial plane in the fluid domain from the pressure inlet to the pressure outlet into  $Q_1Q_2$ ,  $Q_2Q_3$  and  $Q_3Q_4$ , and randomly and continuously selecting 20, 120 and 550 sample points from each segment in turn according to the arrow direction respectively. The pressure of the sample points on the line segments of 4.0, 4.5, 5.0, 5.5, and 6.0 kPa were recorded as shown in Fig. 6 f. In the process of airflow from  $Q_1$  to  $Q_2$ , the vertical section area of the line segment is basically unchanged. The pressure shows a downward trend, but the downward speed gradually slows down. The inlet pressure of 4.0, 4.5, 5.0, 5.5, 6.0 kPa decreased by 292.83, 310.76, 359.53, 406.06 and 437.51 Pa, respectively, and the higher the inlet pressure, the more the pressure decreased. In the process of the airflow from  $Q_2$  to  $Q_3$ , the vertical sectional area of the line segment of the sample points before and after  $Q_2$  suddenly changes from small to large. The vertical sectional area of the line segment of the sample points before and after  $Q_3$  suddenly changes from large to small. The pressure first increases slowly, then fluctuates slowly, and finally decreases rapidly. The pressure inlet of 4.0, 4.5, 5.0, 5.5 and 6.0 kPa reached the maximum pressure of this segment at the 42nd, 48th, 54th, 54th and 48th sample points respectively, which are 2974.79, 3405.17, 3783.44, 4227.45 and 4446.06 Pa. During the process of airflow from  $Q_3$  to  $Q_4$ , the vertical cross-sectional area of the line segment remains basically unchanged, and the pressure first rapidly decreases to the lowest point of the entire flow field sample point. The inlet pressure of 4.0, 4.5, 5.0, 5.5, and 6.0 kPa reaches the minimum value at sample points 189, 189, 189, 184, and 185, respectively, which are -679.32, -828.05, -820.72, -1053.8, and -1153.51 Pa, and then shows an upward trend but the upward speed gradually slows down, reaching a local maximum before slowly decreasing again. Each inlet pressure at the 690th sample point is 0 Pa.

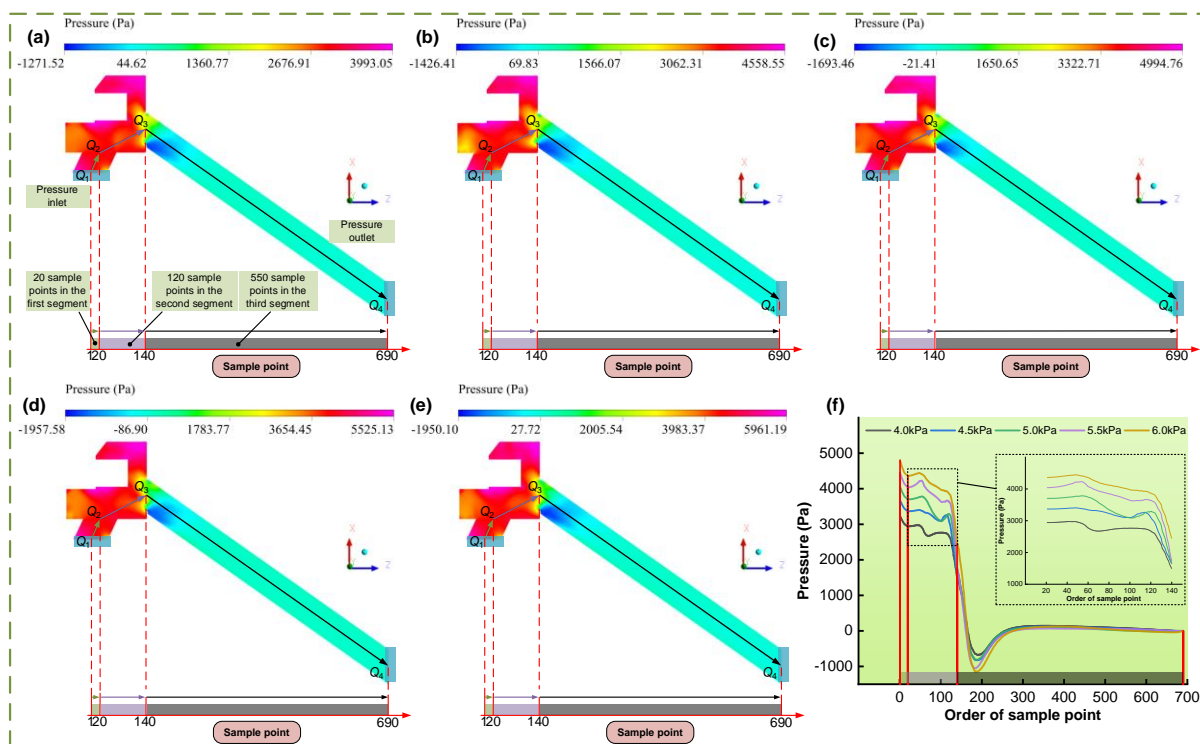


**Fig. 6 - Pressure situation of the airflow seed delivery zone under different inlet pressures**

a. pressure inlet=4.0 kPa; b. pressure inlet=4.5 kPa; c. pressure inlet=5.0 kPa; d. pressure inlet=5.5 kPa; e. pressure inlet=6.0 kPa; f. sample point pressure curve of different inlet pressures.

In order to explore the velocity distribution under different inlet pressures in the airflow seed delivery zone, the axial plane velocity nephogram of the fluid domain at 2 s was intercepted, as shown in Fig. 7 a ~ e. In the figure, with the increase of inlet pressure, the maximum velocity of the whole flow field shows a gradual upward trend, and the maximum velocity reaches 88.61 m/s when the inlet pressure is 6.0 kPa. There was little difference in the velocity distribution of the axial plane under different inlet pressures, and the highest velocity appeared at the outlet pipe, which was caused by the sudden decrease of the cross-sectional area of the airflow from the seed-supply nozzle to the outlet pipe.

The velocity at the sample points on  $Q_1Q_2$ ,  $Q_2Q_3$  and  $Q_3Q_4$  with inlet pressures of 4.0, 4.5, 5.0, 5.5, 6.0 kPa were recorded as shown in Fig. 7 f. In the process of the airflow from  $Q_1$  to  $Q_2$ , the vertical sectional area of the line segment is basically unchanged, and the velocity shows an upward trend, but the rising speed gradually slows down, which is completely opposite to the pressure change trend in the segment, and conforms to the relationship between the velocity and the pressure in Bernoulli's principle. The  $Q_1Q_2$  segment reaches a maximum velocity of 51.7 m/s at the inlet pressure of 6.0 kPa. In the process of airflow from  $Q_2$  to  $Q_3$ , the velocity of each inlet pressure sample does not change much from the 21st to about the 50th sample points, and then it decreases rapidly. The inlet pressures of 4.0, 4.5, 5.0, 5.5, and 6.0 kPa reach the local minimal of the velocity of this segment at the 68th, 61st, 66th, 58th, and 65th sample points, respectively, which are 23.23, 19.52, 28.32, and 22.94, 29.1 m/s. After which the velocity roughly shows a trend of first rising, then falling and then rising. The inlet pressures of 4.0, 4.5, 5.0, 6.0 kPa reach the minimum velocity in this segment at the 111th, 113th, 118th, 115th sample points, respectively, which are 13.62, 16.7, 17.39, and 23.75 m/s. In the process of the airflow from  $Q_3$  to  $Q_4$ , the velocity first rises rapidly to the maximum of the whole flow field sample points. The inlet pressures of 4.0, 4.5, 5.0, 5.5, and 6.0 kPa reach the maximum velocity at the 168th, 164th, 168th, 168th and 168th sample points, respectively, which are 65.66, 64.71, 72.9, 78.88 and 79.4 m/s, and then decreased rapidly. Among them, the inlet pressure of 4.0 kPa and 5.0 kPa decreased relatively slowly, and the inlet pressure of 4.5 kPa was the lowest value of 16.74 m/s at the 229th sample point. The velocity of the sample points before and after the lowest value fluctuated greatly. Finally, the velocity showed an upward trend, but the rising speed gradually slowed down. The velocities at the 690th sample point were 47.68, 52.64, 60.21, 56.8 and 64.82 m/s at the inlet pressures of 4.0, 4.5, 5.0, 5.5, 6.0 kPa, respectively.

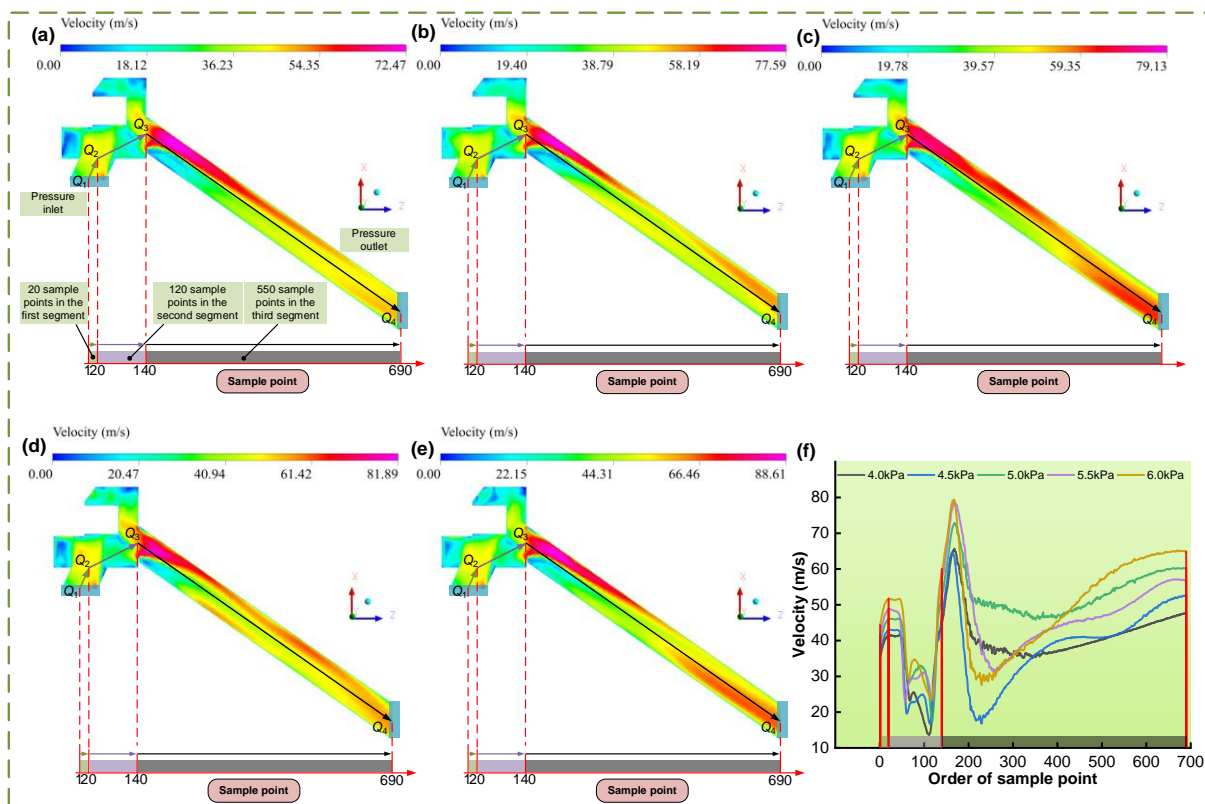


**Fig. 7 - Velocity situation of the airflow seed delivery zone under different inlet pressures**  
 a. pressure inlet=4.0 kPa; b. pressure inlet=4.5 kPa; c. pressure inlet=5.0 kPa; d. pressure inlet=5.5 kPa;  
 e. pressure inlet=6.0 kPa; f. sample point velocity curve of different inlet pressures.

**Results of the multi-factor experiments**

According to the range of factors in Table 2, a multi-factor test was conducted, and the test results are shown in Table 3. In the table,  $X_1$ ,  $X_2$ , and  $X_3$  are coded values of seed supply rate, coefficient of variation of seed supply rate stability, and seed breakage rate, respectively. The test results were processed and analyzed by Design-Expert 12 software, and the quadratic equation variance analysis was obtained as shown in Table 4.

Table 3

| Design and results of the Central-Composite experiment |                      |                        |                         |       |       |
|--|----------------------|------------------------|-------------------------|-------|-------|
| No.  | Experimental factors |                        | Experiment indexes      |       |       |
|  | X1/ kPa              | X2/ km·h <sup>-1</sup> | Y1/ g·min <sup>-1</sup> | Y2/ % | Y3/ % |
| 1  | -1                   | -1                     | 1390.15                 | 1.64  | 1.22  |
| 2  | 1                    | -1                     | 2152.24                 | 1.05  | 1.51  |
| 3  | -1                   | 1                      | 1833.94                 | 1.61  | 1.46  |
| 4  | 1                    | 1                      | 2676.8                  | 1.54  | 1.58  |
| 5  | -1.414               | 0                      | 1448.44                 | 1.94  | 1.3   |
| 6  | 1.414                | 0                      | 2554.86                 | 1.16  | 1.62  |
| 7  | 0                    | -1.414                 | 1670.56                 | 1.15  | 1.36  |
| 8  | 0                    | 1.414                  | 2402.78                 | 1.89  | 1.56  |
| 9  | 0                    | 0                      | 2017.56                 | 1.65  | 1.48  |
| 10   | 0                    | 0                      | 2007.56                 | 1.58  | 1.43  |
| 11   | 0                    | 0                      | 2001.99                 | 1.52  | 1.44  |
| 12   | 0                    | 0                      | 2002.98                 | 1.59  | 1.47  |
| 13   | 0                    | 0                      | 2043.70                 | 1.69  | 1.49  |
| 14   | 0                    | 0                      | 2030.79                 | 1.72  | 1.39  |
| 15   | 0                    | 0                      | 2008.34                 | 1.51  | 1.37  |
| 16   | 0                    | 0                      | 2022.48                 | 1.71  | 1.42  |

Table 4

| Variance analysis of the regression model |                  |            |  |          |                    |            |
|---|------------------|------------|--|----------|--------------------|------------|
| Source                                    | Seed supply rate |            | Coefficient of variation of seed supply rate stability |          | Seed breakage rate |            |
|   | Sum of squares   | p-value    | Sum of squares   | p-value  | Sum of squares     | p-value    |
| Model                                     | 1.761E+06        | < 0.0001** | 0.8020   | 0.0005** | 0.1451             | < 0.0001** |
| X1  | 1.256E+06        | < 0.0001** | 0.3886   | 0.0003** | 0.0930             | < 0.0001** |
| X2  | 5.019E+05        | < 0.0001** | 0.2837   | 0.0008** | 0.0439             | 0.0002**   |
| X1 X2                                     | 1630.95          | 0.0251*    | 0.0676   | 0.0439*  | 0.0072             | 0.0446*    |
| X1 <sup>2</sup>                           | 663.32           | 0.1242     | 0.0237   | 0.2027   | 0.0005             | 0.5795     |
| X2 <sup>2</sup>                           | 565.05           | 0.1524     | 0.0385   | 0.1126   | 0.0005             | 0.5795     |
| Residual                                  | 2354.41          |            | 0.1273   |          | 0.0137             |            |
| Lack of fit                               | 835.36           | 0.3523     | 0.0788   | 0.0666   | 0.0009             | 0.9134     |
| Pure error                                | 1519.06          |            | 0.0485   |          | 0.0128             |            |
| Cor total                                 | 1.763E+06        |            | 0.9293   |          | 0.1588             |            |

Note: \* indicates a significant impact; \*\* indicates a highly significant impact.

In Table 4, the  $p$  values of the regression models of seed supply rate  $Y1$ , Coefficient of variation of seed supply rate stability  $Y2$ , and seed breakage rate  $Y3$  were all less than 0.01, indicating that the regression models were extremely significant. The  $p$ -values of the lack of fit test were all more than 0.05, indicating that the regression models had good fit. In the variance analysis of the  $Y1$ ,  $Y2$  and  $Y3$ , the blower pressure  $X1$  and rotational speed of spiral shaft  $X2$  showed extremely significant effects, and the interaction  $X1 X2$  showed significant effects. The influence order of each factor on the  $Y1$ ,  $Y2$  and  $Y3$  was:  $X1$ ,  $X2$ . The quadratic regression equation of  $Y1$ ,  $Y2$  and  $Y3$  is as follows:

$$\begin{cases} Y1 = -1584.37 + 567.44X1 + 0.44X2 + 2.69X1X2 - 18.21X1^2 + 0.075X2^2 \\ Y2 = 2.33 - 0.35X1 + 0.011X2 + 0.017X1X2 - 0.11X1^2 - 0.00062X2^2 \\ Y3 = -0.97 + 0.37X1 + 0.027X2 - 0.0057X1X2 + 0.015X1^2 + 0.000067X2^2 \end{cases} \quad (8)$$

In order to explore the influence trend of interaction terms of factors on the  $Y1$ ,  $Y2$  and  $Y3$ , the contour map is drawn as shown in Fig. 8.

In Fig. 8a, when the rotational speed is constant, the  $Y1$  is positively correlated with the blower pressure. The greater the pressure, the faster the conveying velocity of maize seeds entrained by airflow, the shorter the conveying time, and the higher the seed supply rate. When the pressure is constant, the  $Y1$  is positively correlated with the rotational speed. The increase of the rotational speed can improve the migration velocity of the seeds in the migration zone, thereby improving the seed supply rate of the device. When the

pressure is 5.75~6.0 kPa and the rotational speed is 75~80 r/min, the  $Y1$  is relatively high, ranging from 2712.86 to 2975 g/min. In Fig. 8b, when the rotational speed is constant, the  $Y2$  is negatively correlated with the pressure at the rotational speed of 50 ~ 75 r/min, and it increases slowly at first and then decreases with the increase of the pressure at the rotational speed of 75 ~ 80 r/min. When the pressure was constant, the  $Y2$  increased first and then decreased with the increase of the rotational speed at the pressure of 4.0~4.6 kPa, and it was roughly positively correlated with the rotational speed at the pressure of 4.6~6.0 kPa. When the pressure is 5.75~6.0 kPa and the rotational speed is 50~52.5 r/min, the  $Y2$  is relatively low, ranging from 0.53 % to 0.83 %. In Fig. 8c, when the rotational speed is constant, the  $Y3$  is positively correlated with the pressure. The higher the pressure, the faster the airflow entraps the seeds in the airflow seed delivery zone, and the easier it is to cause damage to the seeds coating when the seed collides with the seed and the seed collides with the inner wall of the device. When the pressure was constant, the  $Y3$  was positively correlated with the rotational speed. With the increase of the rotational speed, the disturbance effect of the spiral shaft on the seed cluster in the migration zone is more obvious. The frequency of friction between seeds and seeds, seeds and components in the migration zone is increased. At the same time, with the increase of the rotational speed, the inertia force when the seeds flow out from the migration zone also increases, and the collision between the seeds and the seed-supply nozzle is intensified under the action of airflow. When the pressure is 4.0~4.25 kPa and the rotational speed is 50~55 r/min, the  $Y3$  is relatively low, ranging from 1.12 % to 1.25 %.

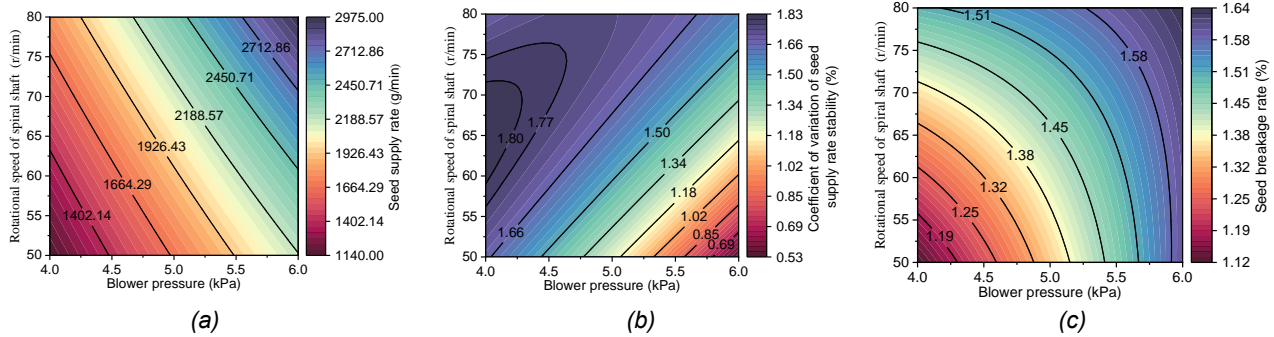


Fig. 8 - Effect of interactivity on test index

According to the results of multi-factor experiments, the optimal working parameter combination of the device was determined based on the multi-objective variable optimization method. With the highest  $Y1$ , the lowest  $Y2$  and  $Y3$  as the optimization objectives, the optimization equation is established within the range of factors and solved by Design-Expert 12 software.

The optimization equation is as follows:

$$\left\{ \begin{array}{l} \max Y1 \\ \min Y2 \\ \min Y3 \\ s. t. \left\{ \begin{array}{l} 4\text{kPa} \geq X1 \geq 6\text{kPa} \\ 50\text{r/min} \geq X2 \geq 80\text{r/min} \\ 1 \geq Y2(X1, X2) \geq 0 \\ 1 \geq Y3(X1, X2) \geq 0 \end{array} \right. \end{array} \right. \quad (9)$$

After calculation, the optimal working parameter combination for the device is: the pressure and the rotational speed are 6.0kPa and 80r/min, respectively. Under this parameter combination, the  $Y1$ ,  $Y2$ , and  $Y3$  are 2971.515 g/min, 1.774 %, and 1.616 %, respectively. The results were verified by bench test, and the  $Y1$ ,  $Y2$ , and  $Y3$  were 2933.21 g/min, 1.87 %, and 1.69 %, respectively, with the relative error of less than 5.5 % compared to the parameter optimization results. The optimized combination of working parameters makes the device achieve better test results in the bench test, and the error is small, which shows that the parameter optimization is effective.

**CONCLUSIONS**

In this study, according to the working process, the air-assisted spiral seed-supply device was divided into the migration zone and the airflow seed delivery zone. By establishing the kinetic model of maize seeds in the migration zone, the theoretical relationship between the absolute angular velocity  $\omega_a$  of the seed cluster microsegment and the angular velocity  $\omega_s$  of the spiral shaft was obtained. Based on the CFD simulation, when the inlet pressure of the airflow seed delivery zone at 2 s was 4.0, 4.5, 5.0, 5.5 and 6 kPa, the pressure range

was -1271.52 ~ 3993.05, -1426.41 ~ 4558.55, -1693.46 ~ 4994.76, -1957.58 ~ 5525.13, -1950.10 ~ 5961.19 Pa, and the maximum velocity of the airflow was 88.61 m/s. Based on the CCD, the multi-factor experiment was carried out, and the influence order of blower pressure  $X_1$  and rotational speed of spiral shaft  $X_2$  on seed supply rate, coefficient of variation of seed supply rate stability and seed breakage rate was:  $X_1$ ,  $X_2$ . Based on the multi-objective variable optimization method, the optimal working parameter combination of the device was determined as the blower pressure of 6.0 kPa and the rotational speed of spiral shaft of 80 r/min. Under the verification test, the seed supply rate, the coefficient of variation of seed supply rate stability and the seed breakage rate were 2933.21 g/min, 1.87% and 1.69%, respectively. The relative error is within 5.5% compared with the result of parameter optimization. The device obtains higher seed supply performance under the optimized working parameter combination.

## ACKNOWLEDGEMENT

The study was funded by the Heilongjiang Province Key Research and Development Program Major Projects, China (2022ZX05B02) and Ltd. 2023 Pilot Project on Integration of Agricultural Machinery R&D, Manufacturing, and Promotion and Application.

## REFERENCES

- [1] Chen, X., Luo, X., Wang, Z., Zhang, M., Hu, L., Yang, W., Zeng, S., Zang, Y., Wei, H., & Zheng, L. (2015). Design and experiment of a fertilizer distribution apparatus with double-level screws. *Transactions of the Chinese Society of Agricultural Engineering*, Vol. 31, Issue 3, pp. 10-16. <https://doi.org/10.3969/j.issn.1002-6819.2015.03.002>
- [2] Ding, Y., Wang, K., Liu, X., Liu, W., Chen, L., Liu, W., & Du, C. (2021). Research progress of seeding detection technology for medium and small-size seeds. *Transactions of the Chinese Society of Agricultural Engineering*, Vol. 37, Issue 8, pp. 30-41. <https://doi.org/10.11975/j.issn.1002-6819.2021.08.004>
- [3] Fanigliulo, R., Grilli, R., Benigni, S., Fornaciari, L., Biocca, M., & Pochi, D. (2022). Effect of sowing speed and width on spacing uniformity of precision seed drills. *INMATEH-Agricultural Engineering*, Vol. 66, Issue 1, pp. 9-18. <https://doi.org/10.35633/inmateh-66-01>
- [4] Gao, X., Xie, G., Xu, Y., Yu, Y., & Lai, Q. (2022). Application of a staggered symmetrical spiral groove wheel on a quantitative feeding device and investigation of particle motion characteristics based on DEM. *Powder Technology*, Vol. 407, pp. 117650. <https://doi.org/10.1016/j.powtec.2022.117650>
- [5] Gao, X., Xu, Y., Yang, L., Zhang, D., Li, Y., & Cui, T. (2018). Simulation and experiment of uniformity of venturi feeding tube based on DEM-CFD Coupling. *Transactions of the Chinese Society of Agricultural Machinery*, Vol. 49, Issue S1, pp. 92-100. <https://doi.org/10.6041/j.issn.1000-1298.2018.S0.013>
- [6] Huai, H., Zhang, Q., Liu, M., & Tang, X. (2024). Changes in climate attributes and harvest area structures jointly determined spatial-temporal variations in water footprint of maize in the Beijing-Tianjin-Hebei region. *Heliyon*, Vol. 10, Issue 12, pp. E32565. <https://doi.org/10.1016/j.heliyon.2024.e32565>
- [7] Lei, X., Liao, Y., Wang, L., Wang, D., Yao, L., & Liao, Q. (2017). Simulation of gas-solid two-phase flow and parameter optimization of pressurized tube of air-assisted centralized metering device for rapeseed and wheat. *Transactions of the Chinese Society of Agricultural Engineering*, Vol. 33, Issue 19, pp. 67-75. <https://doi.org/10.11975/j.issn.1002-6819.2017.19.009>
- [8] Sun, W., Yi, S., Qi, H., Dai, Z., Zhang, Y., & Wang, S. (2024). Research progress on narrow row and dense planting delta-row seeding technology and equipment. *Agricultural Engineering*, Vol. 14, Issue 5, pp. 5-9. <https://doi.org/10.19998/j.cnki.2095-1795.2024.05.001>
- [9] Sun, W., Yi, S., Qi, H., Li, Y., Dai, Z., Zhang, Y., & Wang, S. (2024). Design and experiment of progressive seed-cleaning mechanism for air-pressure maize precision seed-metering device. *INMATEH-Agricultural Engineering*, Vol. 73, Issue 2, pp. 473-486. <https://doi.org/10.35633/inmateh-73-40>
- [10] Tang, H., Guan, T., Xu, F., Xu, C., & Wang, J. (2024). Test on adsorption posture and seeding performance of the high-speed precision dual-chamber maize metering device based on the seed characteristics. *Computers and Electronics in Agriculture*, Vol. 216, pp.108471. <https://doi.org/10.1016/j.compag.2023.108471>
- [11] Wang, L., Liao, Y., Liao, Q., Qi, T., Zhang, Q., & Wang, B. (2021). Design and test on centralized metering seed feeding device of air-assisted planter for rapeseed. *Transactions of the Chinese Society of Agricultural Machinery*, Vol. 52, Issue 2, pp.75-85. <https://doi.org/10.6041/j.issn.1000-1298.2021.02.007>

- [12] Wang, L., Liao, Y., Zhang, Q., Liu, H., Wang, B., & Liao, Q. (2020). Experiments and analysis on seeding performance of seed feeding device of rapeseed centralized metering device under lateral tilt. *Transactions of the Chinese Society of Agricultural Engineering*, Vol. 36, Issue 19, pp.1-10. <https://doi.org/10.11975/j.issn.1002-6819.2020.19.001>
- [13] Yao, L., Liao, Q., Wang, L., Liu, H., Wei, G., & Wang, B. (2022). Design and experiment of spiral seed feeding device in spinning disc high-speed metering device for rapeseed. *Transactions of the Chinese Society of Agricultural Machinery*, Vol. 53, Issue 6, pp. 78-88. <https://doi.org/10.6041/j.issn.1000-1298.2022.06.008>
- [14] Yang, W., Fang, L., Luo, X., Li, H., Ye, Y., & Liang, Z. (2020). Experimental study of the effects of discharge port parameters on the fertilizing performance for fertilizer distribution apparatus with screw. *Transactions of the Chinese Society of Agricultural Engineering*, Vol. 36, Issue 17, pp.1-8. <https://doi.org/10.11975/j.issn.1002-6819.2020.17.001>
- [15] Yuan, H., Liu, C., Song, J., Du, X., Jiang, M., & Li, W. (2020). Piezoelectric vibration seed supply device of precision metering device for plug seedling of super hybrid rice. *Transactions of the Chinese Society for Agricultural Machinery*, Vol. 51, Issue S2, pp. 31-40. <https://doi.org/10.6041/j.issn.1000-1298.2020.S2.004>